Pageoph, in press

(2)

Rupture directivity during the September 7, 1999 (M_w 5.9) Athens (Greece) earthquake obtained from strong motion records

Z. Roumelioti[1], A. Kiratzi[1], N. Theodoulidis[2], I. Kalogeras[3] and G. Stavrakakis[3]

[1] *Department of Geophysics, Aristotle University of Thessaloniki, 54006 Thessaloniki, Greece.*
[2] *Institute of Engineering Seismology and Earthquake Engineering, P.O. Box 53, 55102, Thessaloniki, Greece.*
[3] *Institute of Geodynamics, National Observatory of Athens, P.O. Box 20048, 11810, Athens, Greece.*

ABSTRACT

The empirical Green's functions technique is applied to simulate strong ground motion records from the September 7, 1999, Athens earthquake. Information on the fault parameters from previous independent studies has been used and several scenarios were examined, in regard to the location of starting point of the rupture, by comparing the synthetic records with the corresponding observed ones, through a residual function and a correlation function. The results show that the rupture started at the deepest, ~ 4–5 Km, part of the fault, from its western edge. This hypocenter was then used, in combination with the initial fault model, to stochastically simulate the strong ground motion during the Athens mainshock, in terms of peak ground acceleration at hard rock. The results show that directivity might have significantly contributed to the destructiveness of this earthquake at specific parts of the Athens metropolitan area.

Keywords: rupture directivity, ground motion, Athens, Greece

Introduction

On September 7, 1999, at 11:56 GMT (14:56 local time), a strong earthquake of magnitude M_w 5.9 occurred very close to the capital of Greece, Athens. This event, the first reported at such close distance from the center of Athens (~18 Km), at least during instrumental time, caused the death of 143 people and the collapse of ~100 buildings, among which some industrial buildings. The heaviest damage occurred at the northern suburbs of Athens, close to the epicentral area, where maximum intensity was estimated to be of the order of IX (modified Mercalli–Sieberg scale).

So far, much discussion has been done about the fault of the Athens earthquake and the causes of the extensive structure failures close to the epicenter. The earthquake fault did not produce any typical surface traces and so it was difficult to relate it to previously mapped faulting or to clearly define its trace on the surface. Nevertheless, some ground failures (Pavlides et al., 2000) were observed along the Fili neotectonic fault (figure 1), indicating a possible relation of the particular fault to the Athens mainshock.

Relatively to the causes of the heavy damage reported at the northern suburbs of Athens, factors such as local site conditions, poor foundation conditions, topographic effects etc. have been mentioned based on information collected during fieldwork (Anastasiadis et al., 1999; Psycharis et al., 1999). Nevertheless, there is no detailed information about these factors since they are still under examination.

In the present work, we examine the role of directivity during the September 7, 1999, Athens mainshock in its devastating consequences. A major obstacle towards this direction is the uncertainty in the location of the hypocenter on the fault plane. Therefore, we first apply the empirical Green's

function (EGF) technique of Irikura (1983) in an examination of the optimum location for the hypocenter. The result is then used in combination with other fault parameters, such as fault length and width, from independent studies, to simulate the strong ground motion during the Athens earthquake. The results are shown in terms of peak ground acceleration at hard rock.

Examination of the Hypocenter Location by the EGF Method

We applied the methodology of Irikura (1983, 1986) to simulate the strong ground motion from the Athens mainshock (M_w=5.9), using seven records of three of its aftershocks as empirical Green's functions. The epicenters of the aftershocks used in this study are shown along with the epicenter of the simulated mainshock and the recording stations in fig. 1. The source parameters of these earthquakes are listed in Table 1. Epicenters are taken from Papadopoulos et al. (2000), while magnitudes are taken from the on–line catalog of the National Observatory of Athens (*http://www.gein.noa.gr*). In Table 2 we present some information on the recording stations mentioned in this study.

We must point out that the data used as empirical Green's functions have many disadvantages: their magnitudes are relatively small compared to the target event (M_w 3.7 and M_w 3.8) and their epicenters are located at the eastern part of the area covered by the aftershock activity, being relatively away from the epicenter of the mainshock. Furthermore, because of the small magnitudes the errors in the employed source parameters may be large. So, the aim of the simulations is not to obtain the best synthetics at each site, but to examine the relative performance of different EGF's at revealing information about the position of the rupture starting point. In other words, we do not examine the

synthetics in terms of the goodness of fit with the observed records of the mainshock, but we investigate the existence of resemblances in the inferred rupture process.

Methodology

The methodology is based on a combination of the EGF technique (Hartzell, 1978) with the similarity law of earthquakes and has been repeatedly described in previous works (e.g., Irikura, 1983, 1986; Kamae and Irikura, 1994).

According to Kamae and Irikura (1994), when two events occur within the same seismic source, the similarity law of earthquakes can be briefly described by the equation:

$$\frac{L}{L_e} = \frac{W}{W_e} = \frac{D}{CD_e} = \frac{\tau}{\tau_e} = \left(\frac{M_0}{CM_{0e}} \right)^{\frac{1}{3}} = N \qquad (1)$$

Parameters without subscript are for the larger event and those with subscript, e, are for the smaller event. L and W are the length and width of the fault, respectively, D is the final offset of the dislocation, ô is the rise time and M_0 is the scalar seismic moment. C stands for the ratio of stress drop, Äó, between the two events:

$$C = \frac{\Delta\sigma}{\Delta\sigma_e} \qquad (2)$$

and N is a scaling parameter used to discretize the fault, defined as the closest integer to the value calculated from the equation:

$$N = \left(\frac{M_0}{C \cdot M_0} \right)^{\frac{1}{3}} \qquad (3)$$

Parameters C and N are of great importance for the simulations since the first one controls the level of the simulated spectrum and the second one defines the number of elements (N×N) in which the target fault is subdivided. In the case of the ù–square spectral scaling model, the above parameters can be estimated from the relations (Kamae and Irikura, 1994):

$$\frac{U_0}{U_{0e}} = \frac{M_0}{M_{0e}} = CN^3 \tag{4}$$

and

$$\frac{A_0}{A_{0e}} = CN \tag{5}$$

where U_0 and A_0 correspond to the flat level of the displacement spectrum and the flat level of the acceleration spectrum, respectively. An alternative way to estimate the above parameters is through the use of empirical scaling relations instead of spectral scaling relations (Roumelioti et al., 2000), or from independent methods such as the spectral analysis.

The synthetic record is finally estimated by summing up the contributions from all subfaults, appropriately lagged in time.

Modeling parameters

The length, L, and width, W, of the target fault were taken equal to 15 Km and 10 Km, respectively (Papadimitriou et al., 2000). These values are in very good agreement with those expected from the empirical scaling relations applicable to Greece (Papazachos and Papazachou, 1997) and quite close to those defined by the distribution of the aftershock epicenters (Papazachos et al., 2000) and by a spectral analysis of teleseismic data carried out by Louvari and Kiratzi (2001).

Parameters C and N were estimated from relations (2) and (3), respectively. The seismic moment of the mainshock was taken equal to 9.0×10^{24} dyn·cm (Louvari and Kiratzi, 2001). The seismic moments of the small earthquakes were taken from Stavrakakis et al. (2001), along with the source dimension, r, of the EGF's and the mainshock (Table 3). The stress drop, Äó, was estimated based on the relation of Keilis–Borok (1959) between stress drop, seismic moment and the radius of the seismic fault, r:

$$\Delta\sigma = \frac{7M_0}{16r^3} \qquad (6)$$

Following relations (2), (3) and (6), the parameters C and N are estimated, as shown in Table 3, for each one of the three small events used as empirical Green's functions.

The rise time of either the small or the large event can be estimated from empirical relations (e.g., Geller, 1976). Nevertheless, for the Athens mainshock, there is evidence of very short rise time, 0.1–0.3 sec (Tselentis and Zahradnik, 2000; Louvari and Kiratzi, 2001). Therefore we preferred to use the value of 0.3 sec for the target event, instead of computing it from empirical relations.

The modeling parameters used in the EGF simulations are summarized in Table 3. Parameters related to the focal mechanism of each event are taken from Papadopoulos et al. (2000).

The examination of the location of the rupture nucleation was carried out by keeping the dimensions of the fault fixed and performing simulations for several scenarios. We examined 16 different scenarios by successively assigning the hypocenter at each one of the marked sub-elements depicted in fig. 2. The measures that we used to evaluate the relative performance of the simulations

were the correlation function, *ö*, and the residual function, *res*, which can be described by the equations (Irikura, 1983):

$$\phi = \left[\int_0^T f(t') \cdot g(t-t')dt' \Big/ \left(\int_0^T f^2(t)dt \cdot \int_0^T g^2(t)dt \right)^{\frac{1}{2}} \right] \tag{7}$$

and

$$res = \int_0^T (f-g)^2 dt \Big/ \left(\int_0^T f^2 dt \cdot \int_0^T g^2 dt \right)^{\frac{1}{2}} \tag{8}$$

where f(t) and g(t) are the synthesized and observed records, respectively, and T is the time window of the examined data.

The values obtained for the residual function and the correlation function for the longitudinal component (results for the other two components are similar) are mapped in fig. 2. Areas on the fault plane of lowest residuals are depicted in white color (left part of figure 2) while areas that are less favorable to have included the hypocenter are depicted in dark colors. On the contrary, areas on the fault plane with highest correlation functions are depicted with dark colors, while the lowest values are the whiter ones. For each pair of maps, we also note the station at which we performed the simulations and the employed EGF. All the examined pairs of "target event – small event" present lower residuals and higher correlation at the northwestern bottom of the fault and in most cases (fig. 2a, 2b, 2c, 2e, 2g) an even more preferable solution at 4-5 Km from the northwestern bottom edge of the fault. The levels of residual and correlation vary in absolute values (lowest residual vary from 0.45 to 1.15 and highest correlation from 0.44 to 0.82) among the different sets of simulations. These variations could be attributed to many factors such as errors in the employed source parameters, near–field effects, bad quality of empirical Green's functions etc. Nevertheless, the aim of the present study was accomplished since the relative comparison of

the extracted values reveals a consistency of the results regarding the location of the hypocenter.

In figure 3, we indicatively present the observed records of the longitudinal component at the four stations used in this study, together with the simulated waveforms (hypocenter at 5 Km from the northwestern bottom edge of the fault). The number of simulations at each station depends on the available records of the three EGFs. Despite the previously mentioned disadvantages of the empirical Green's functions used, in some cases the observed records are satisfactorily reproduced (e.g. the observed record at ATHA by using event B as EGF). Even in cases where different phases are not well synthesized (e.g. figure 3d), the spectral fit is quite good (figure 4).

Forward Modeling of Strong Ground Motion by the Stochastic Method

The optimum location of the hypocenter derived from the EGF simulations was used as input in a stochastic strong ground motion simulation, to produce synthetic peak ground accelerations for hard rock sites during the 1999 Athens earthquake. The purpose of this part of our work was to examine whether the inferred by the EGF simulations fault model can predict the areas of strong shaking during the Athens mainshock.

Methodology

The employed method is the stochastic method for finite sources (Beresnev and Atkinson, 1997, 1998, 1999). In this method, the seismic radiation from a finite fault is derived by dividing the fault into a certain number of equal

rectangular elements (subfaults), which also have finite dimensions ÄlxÄw, and summing their contributions at the observation point. According to Beresnev and Atkinson (1999), the optimum subfault size, Äl, is linearly related to moment magnitude, M_w, of the simulated event and can be defined by the relation:

$$\log \Delta l = -2 + 0.4 M_w \tag{9}$$

Each subfault is treated as a point source with an underlying ù–square spectrum, which can be fully determined by two parameters: the seismic moment and the corner frequency, f_c. These two parameters are connected to the finite subfault dimensions through the coefficients Äó and ê. In detail, in the simple case for which Äl=Äw, the subfault moment (m_0) is related to Äl through coefficient Äó, following the relation:

$$m_0 = \Delta\sigma \cdot \Delta l^3 \tag{10}$$

where Äó is a "stress parameter", most closely related to the static stress drop (Beresnev and Atkinson, 1998). On the other hand, the corner frequency of the subfault spectrum, f, is related to Äl through coefficient ê, which actually controls the level of the simulated high–frequency radiation. The mathematical expression of this relation is:

$$\kappa = \frac{f_c \cdot \Delta l}{\beta} \tag{11}$$

where â is the shear wave velocity. Coefficient ê can alternatively be estimated by:

$$\kappa = \frac{y \cdot z}{\pi} \tag{12}$$

where y is the ratio of rupture velocity to shear–wave velocity and z stands for the ratio of the rise time of a small finite source to the rise time of an equivalent point source. This latter parameter actually depends on the way that rise time is

defined in the exponential functions that describe the ù–square model (Beresnev and Atkinson, 1997).

According to the pre–mentioned, the application of the finite–fault simulation method requires the definition of parameters that include fault geometry (length, width, strike, dip, depth of the upper edge of the fault), propagation effects (geometric spreading, anelastic attenuation), site effects, subfault size and the "radiation–strength factor", a parameter that can be related to maximum slip velocity. Provided that the fault parameters are known, or controlled by independent studies, the only free parameter of the method is the radiation–strength factor.

Application of the stochastic method

The fault parameters, including dimensions and orientation, were kept the same as in the EGF simulations. So, based on the subfault size estimated from relation (9), the fault was subdivided into 7×4 elements. The rupture initiation point was also considered to coincide with the optimum hypocenter imposed by the deterministic synthetics (at the bottom of the fault, ~5 Km from its northwestern edge).

The radiation strength factor, which consists the only free parameter of the method, was taken equal to 1.7, a value found applicable to Greece (Roumelioti et al., 2000). Other values, obtained from modeling Californian earthquakes, are within 1.0 and 1.6, while in few cases they exceed 2.0.

For the geometric attenuation we employed the model of Raoof et al. (1999) determined from Californian data, while the anelastic attenuation was

represented by a mean frequency–dependent quality factor for the area of Greece, $Q(f) = 100\, f^{0.8}$ (P. Hatzidimitriou, personal communication).

The effect of the near–surface attenuation was also taken into account by diminishing the simulated spectra by the factor $\exp(-\pi f\kappa)$ (Anderson and Hough, 1984). The kappa operator was given a value of 0.035, previously estimated (Margaris and Boore, 1998). Finally, since the synthetics were calculated for hard–rock sites, we included only slight amplifications at high frequencies, by employing the amplification factors for very hard rock proposed by Boore and Joyner (1997). The above modeling parameters are summarized in table 4.

We performed simulations at 20 equally distant (18° interval) azimuths and at distances from 3 to 50 Km (at 3 Km and from 5-50 Km in 5 Km increment) from the center of the fault trace. Since slip distribution during the Athens mainshock is unknown, we repeated the modeling procedure for four different random slip distribution models, generated by the source code used (FINSIM, Beresnev and Atkinson, 1997). These models are shown in fig. 5 (slip values are in meters).

After the completion of the simulations, we calculated the mean peak ground acceleration (pga) at each distance, over the 20 azimuths. Next, we estimated the difference between each synthetic PGA and the mean PGA at the corresponding distance, in terms of % of the mean value.

In figure 6 we present maps of the synthetic peak ground accelerations (left part) and the lateral variations of their differences relative to the mean values (right part). In each map, the fault trace (thick line) and the areas of heaviest damage (solid squares) are also depicted. Dots indicate the observation points.

Even though there are differences among the four sets of results, showing a dependency on the slip distribution model, there are also many common characteristics on the distribution of strong motion. The maximum absolute values of pga are systematically concentrated within the projection of the fault and even though the simulations were performed for a moderate earthquake and for hard rock sites, they locally exceed 0.5g. On the other hand, the values on the footwall are lower and they seem to decrease more rapidly with distance.

All models indicate a clear directivity towards E-SE, at least up to distances ~20 Km. The azimuthal distribution of strong ground motion is better showed at the right part of figure 6. In these maps, areas of increased pga are depicted with white color, while areas of low pga are shown in dark gray. Light gray covers areas where the simulated peak values indicate either an increase or decrease, which nevertheless lies within the range of ±1 standard deviation of the estimated mean pga at each azimuth. In some cases, the mapped differences reach levels as high as 60–80% of the mean value. These increments can be proved particularly catastrophic at distances close to the fault trace, where the levels of strong ground motion are normally high. So, an interesting observation is that the areas of heaviest damage, during the 1999 Athens earthquake, lie within or very close to the white areas. This means that, among other parameters such as site effects, directivity might have been a significant contributor to the devastating consequences of this earthquake.

Conclusions

We applied the EGF method to investigate the rupture initiation point on the fault plane of the September 7, 1999, (M_w 5.9) Athens earthquake. During

this investigation we performed simulations at four strong motion stations, using in total seven records of three aftershocks. For each pair of station – egf we produced 16 synthetics by successively assigning the rupture initiation p oint to different subfaults and keeping the other fault parameters constrained based on independent studies. The comparison between recorded and synthesized waveforms was accomplished through a residual function and a correlation function. Lowest residuals and highest correlation values systematically appear to be consistent with a hypocenter located at the deepest part of the fault model, around 5 Km from its northwestern edge.

Despite the agreement of the results relatively to the location of the hypocenter, the absolute values of the two employed functions correspond to medium levels of fitness between observed and simulated waveforms. This was expected, basically because of the choice of the empirical Green's functions (epicenters relatively away from the mainshock epicenter). Nevertheless, we believe that such levels of prediction or even lower are very likely to be observed in simulations of future events since we have no "a priori" knowledge of either the location of the future hypocenter or the focal mechanism and so we can not choose the closest to the mainshock small events. Therefore, the optimum way of using deterministic simulation methods for future earthquake scenarios, such as the EGF method, should be through the examination of several r upture scenarios and the employment of different small events as empirical Green's functions.

In the second part of our work we used the initial fault model, along with the hypocenter revealed from the EGF synthetics, to stochastically simulate the strong ground motion during the Athens earthquake. Synthetic waveforms were produced at 20 azimuths and at distances from 3–50 Km from the center of the fault trace. Since we did not have any information on the distribution of slip on

the fault, we tested four random slip distribution models. All the examined models revealed an clear increase of the strong ground motion at E–SE of the adopted fault plane. The majority of the heavily damaged areas during the September 7, 1999, Athens earthquake lie within the areas of increased levels of strong motion. This leads us to the conclusion that among other parameters that were not included in the present simulations (e.g site effects), source directivity might have contributed to the increased levels of damage at the northern suburbs of Athens.

Acknowledgements

We would like to thank Prof. I. Beresnev and Prof. K. Irikura for kindly offering the simulation codes. This work was partly financed by Earthquake Planning and Protection Organization (EPPO) of Greece (Contract 20246-2000) and by the Science for Peace Project 972342.

References

Anastasiadis, An., Demosthenous, M., Karakostas, Ch., Klimis, N., Lekidis, B., Margaris, B., Papaioannou, Ch., Papazachos, C. and N. Theodoulidis (1999). The Athens (Greece) earthquake of September 7, 1999: Preliminary report on strong motion data and structural response, *http://www.itsak.gr/report.html*

Anderson, J. and S. Hough (1984). A model for the shape of the Fourier amplitude spectrum of acceleration at high frequencies, *Bull. Seism. Soc. Am.* **74**, 1969 – 1993.

Beresnev, I. A. and G. M. Atkinson (1997). Modelling Finite–Fault Radiation from the ω^n Spectrum, *Bull. Seism. Soc. Am.* **87**, 67 – 84.

Beresnev, I. A. and G. M. Atkinson (1998). FINSIM – a FORTRAN Program for Simulating Stochastic Acceleration Time Histories from Finite Faults, *Seism. Res. Let.* **69**, 27 – 32.

Beresnev, I. A. and G. M. Atkinson (1999). Generic Finite-Fault Model for Ground-Motion Prediction in Eastern North America, *Bull. Seism. Soc. Am.* **89**, 608 – 625.

Boore, D. and W. B. Joyner (1997). Site amplifications for generic rock sites, *Bull. Seism. Soc. Am.* **87**, 327 – 341.

Geller, R. J. (1976). Scaling Relations for Earthquake Source Parameters and Magnitudes, *Bull. Seism. Soc. Am.* **66**, 1501–1523.

Hartzell, S. (1978). Earthquake Aftershocks as Green's Functions, *Geophys. Res. Let.* **5**, 1–4.

Irikura, K. (1983). Semi–Empirical Estimation of Strong Ground Motions during Large Earthquakes, *Bull. Disas. Prev. Res. Inst.* **33**, *Kyoto Univ.*, 63–104.

Irikura, K. (1986). Prediction of strong acceleration motion using empirical Green's function, *Proc. 7th Japan Earthq. Eng. Symp.*, pp. 151-156.

Irikura, K. and K. Kamae (1994). Estimation of strong ground motion in broad frequency band based on a seismic source scaling model and an empirical Green's function technique, *Annali di Geofisica*, **37,** 1721 – 1743.

Keilis–Borok, V. (1959). On the estimation of the displacement in an earthquake source and of source dimensions, *Ann. di Geofis.* **12**, 205–214.

Louvari, E. and A. Kiratzi (2001). Source parameters of the September 7, 1999 Athens (Greece) earthquake from teleseismic data, *J. Balkan Geophys. Soc.*, in print.

Margaris, B. N. and D. M. Boore (1998). Determination of Äó and êo from Response Spectra of Large Earthquakes in Greece, *Bull. Seism. Soc. Am.* **88,** 170–182.

Papadimitriou, P., Kaviris, G., Voulgaris, N., Kassaras, I., Delibasis, N. and K. Makropoulos (2000). The September 7, 1999 Athens earthquake sequence recorded by the Cornet Network: preliminary results of source parameters determination of the mainshock, *Annal. Geolog. de Pays Hel.*,

Papadopoulos, G. A., Drakatos, G., Papanastassiou, D., Kalogeras, I. and G. Stavrakakis (2000). Preliminary results about the catastrophic earthquake of 7 September 1999 in Athens, Greece, *Seism. Res. Let.* **71,** 318 –329.

Papazachos, B. C. and C. Papazachou (1997). The earthquakes of Greece, *Ziti Publ. Co.*, 356 pp.

Papazachos, C. (scientific responsible) (2000). Study of the seismic sequence of Athens earthquake, *Final Report*, pp. 41 (in Greek).

Pavlides, S., Papadopoulos, G. A. and A. Ganas (2000). Seismic hazard in urban areas: The 7th September 1999 Athens earthquake case study, *Proc. Of the Hokudan Int. Symp. and School on Active Faulting: Active Fault Research for the New Millennium,* 17–26 January, 2000, eds: Okumura, K., Takada, K. and H. Goto, 367 – 370.

Psycharis, I., Papastamiou, D., Taflambas, I. and P. Carydis (1999). The Athens, Greece earthquake of September 7, 1999, *EERI Special Earthquake Report, http://www.eeri.org/Reconn/Greece1099*

Raoof, M., Herrmann, R. and L. Malagnini (1999). Attenuation and excitation of three–component ground motion in Southern California, *Bull. Seism. Soc. Am.* **89,** 888 – 902.

Roumelioti, Z., Kiratzi, A., Theodoulidis, N. and Ch. Papaioannou (2000). A comparative study of a stochastic and deterministic simulation of strong ground motion applied to the Kozani – Grevena (NW Greece) 1995 sequence, *Annal. di Geofisica* **43,** N. 5, 951 – 966.

Stavrakakis, G. N., Chouliaras, G. and G. Panopoulou (2001). Seismic source parameters for the M_w=5.9 Athens earthquake (September 7, 1999) from a new telemetric broad-band seismological network in Greece, Natural Hazards, in press.

Tselentis, G–A. and J. Zahradnik (2000). The Athens earthquake of September 7, 1999, *Bull. Seism. Soc. Am.* **90,** 1143 – 1160.

Figure Captions

Figure 1: Regional map showing epicenters of the Athens mainshock (star) and the three aftershocks (solid circles) used as empirical Green's functions. Solid triangles correspond to the strong motion stations used in this study. The dashed line represents the surface projection of the inferred by the EGF simulations fault plane, while the thick continuous line represents the surface trace of the Fili Fault (Papadopoulos et al., 2000).

Figure 2: Examination of the variation of the simulated accelerograms with regard to the location of the rupture starting point. The residual function (left) and the correlation function (right) between synthesized and observed record are mapped on the fault plane. For each pair of maps, we denote the corresponding station name and the event used as EGF. The examined scenarios of the location of the starting point are shown in the upper part of the figure.

Figure 3: Comparison of observed horizontal acceleration time histories (longitudinal component) during the Athens mainshock with the corresponding simulated ones by the EGF method. For each station, the observed record is shown at the left part of the figure, while the synthetic waveforms, derived by the use of different EGFs, are shown at the right.

Figure 4: Comparison between observed spectrum (thick line) and simulated spectrum (thin line) of the longitudinal component at station SGMA.

Figure 5: Random slip distribution models used in the stochastic simulations (methodology of Beresnev and Atkinson, 1997).

Figure 6: Contour maps of the simulated peak ground acceleration (left part) and the lateral variations of the differences between individual estimated values and the mean value at each distance (in terms of % of the mean) (right part), for four scenarios of slip distribution on the fault. Dots correspond to sites where synthetic values have been obtained. The thick continuous line represents the surface projection of the upper edge of the fault model and solid squares correspond to heaviest damaged areas during the Athens mainshock.

Table 1: List of earthquakes used in this study together with their epicentral coordinates, depth and local magnitude (M_L).

Event	**Date** d/m/yr	**Time** h:m:s	**ō°(N)**	**ē°(E)**	**Depth** (Km)	**M_L**
Mainshock	07/09/1999	11:56:51.4	38.08	23.58	16.8	5.4
A	07/09/1999	17:19:21.1	38.11	23.72	16.2	3.8
B	08/09/1999	03:21:32.5	38.09	23.83	14.1	3.7
C	10/09/1999	14:49:57.2	38.08	23.81	9.2	3.7

Table 2: Information on the coordinates and installation sites of the four stations used in this study.

Station	ō°(Í)	ē°(Å)	Site	Building	Geology
ATHA	38.00	23.77	Private building	3-stories RC	Tertiary Deposits
SGMA	37.98	23.74	Metro station	-1 level (-7m)	Schist
SPLA	38.00	23.71	Metro station	-2 level (-13m)	Alluvium - Schist
SPLB	38.00	23.71	Metro garage	3-stories steel building	Manmade

Table 3: Input parameters for the EGF simulations.

Parameter	Target Event	Event A	Event B	Event C
M_w	5.9	4.3	4.2	4.2
M_0 (dyne·cm)	9.22×10^{24}	1.08×10^{22}	6.79×10^{21}	1.55×10^{22}
Epicenter latitude (°)	38.08	38.11	38.09	38.08
Epicenter longitude (°)	23.58	23.72	23.83	23.81
Strike (°)	113	114	106	94
Dip (°)	39	30	26	38
Rake (°)	-90	-87	-74	-90
Hypocentral Depth (Km)	16.8	16.2	14.1	9.2
Rise Time (sec)	0.3	0.043	0.043	0.043
Fault Radius (Km)	5.33	0.77	0.73	0.81
N		7	7	7
C		2.5	3.38	2.0

Table 4: Input parameters for the stochastic simulations.

Parameter	**07/09/1999 Athens Mainshock**
Fault Orientation	Strike 113°, Dip 39°
Fault dimensions (Km)	15×10
Depth to upper edge of the fault (Km)	4
Mainshock moment magnitude (M_w)	5.9
Subfault dimensions (Km)	2.1×2.5
Subfault moment (dyne-cm)	5.67×10^{23}
Number of subfaults	28
Number of subsources summed	14
Subfault corner frequency (Hz)	1.03
Crustal shear-wave velocity (Km/sec)	3.3
Crustal density (gr/cm^3)	2.72
Distance-dependent duration term (sec)	Duration equal to source rise time
Geometric spreading	R^{-1}, R<40Km
	$R^{-0.5}$, R>40Km
Q(f)	$100.0 \times f^{0.8}$
Windowing function	Saragoni-Hart
Kappa operator	0.035

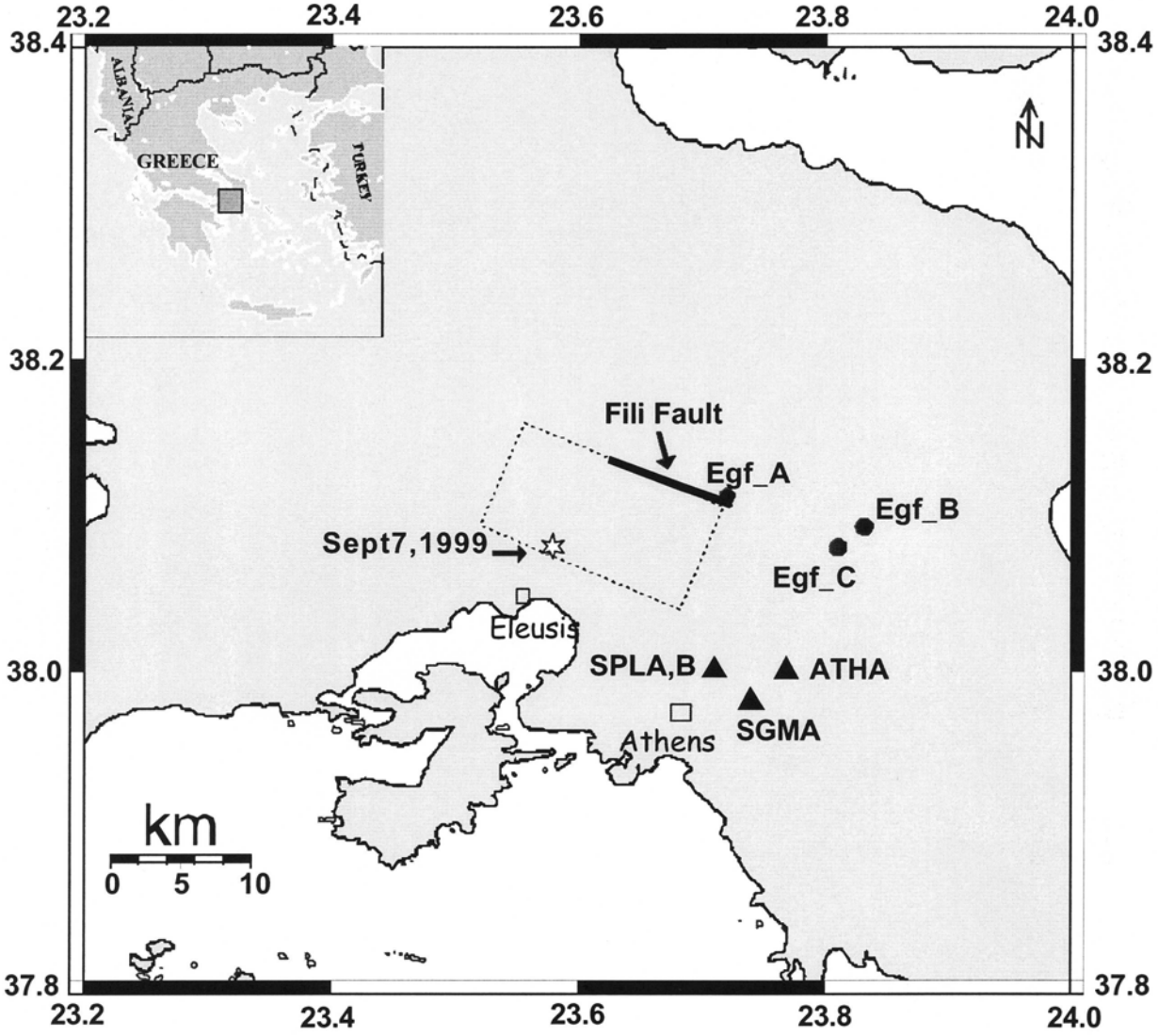
23.2
23.4
23.6
23.8
24.0
38.4
38.2
38.0
37.8
ALBANIA
GREECE
TURKEY
N
Fili Fault
Egf_A
Egf_B
Egf_C
Sept7,1999
Eleusis
SPLA,B
ATHA
SGMA
Athens
km
0 5 10

FIGURE 1

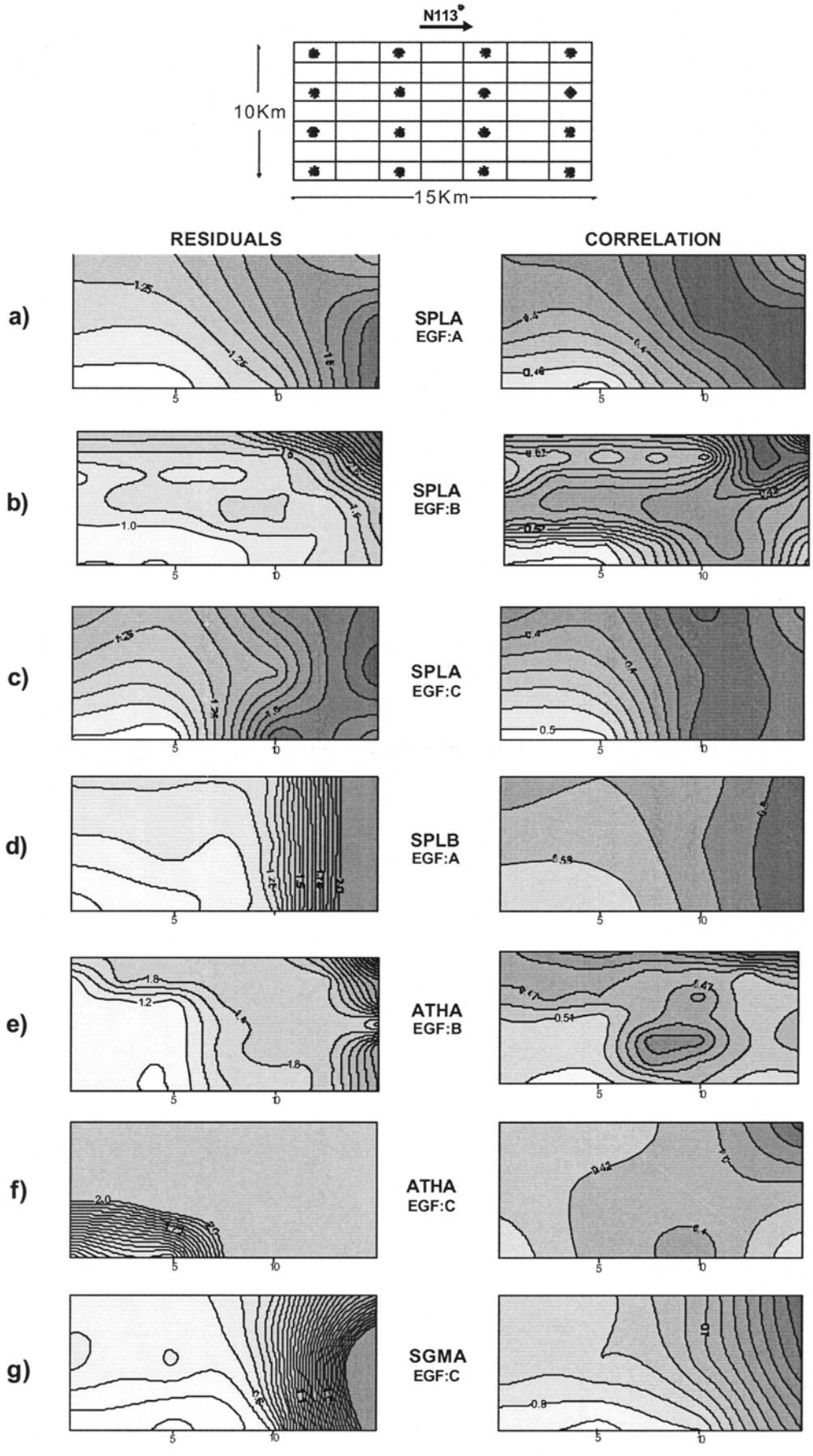
N113°
10Km
15Km
RESIDUALS
CORRELATION
a)
SPLA
EGF:A
b)
SPLA
EGF:B
c)
SPLA
EGF:C
d)
SPLB
EGF:A
e)
ATHA
EGF:B
f)
ATHA
EGF:C
g)
SGMA
EGF:C

FIGURE 2

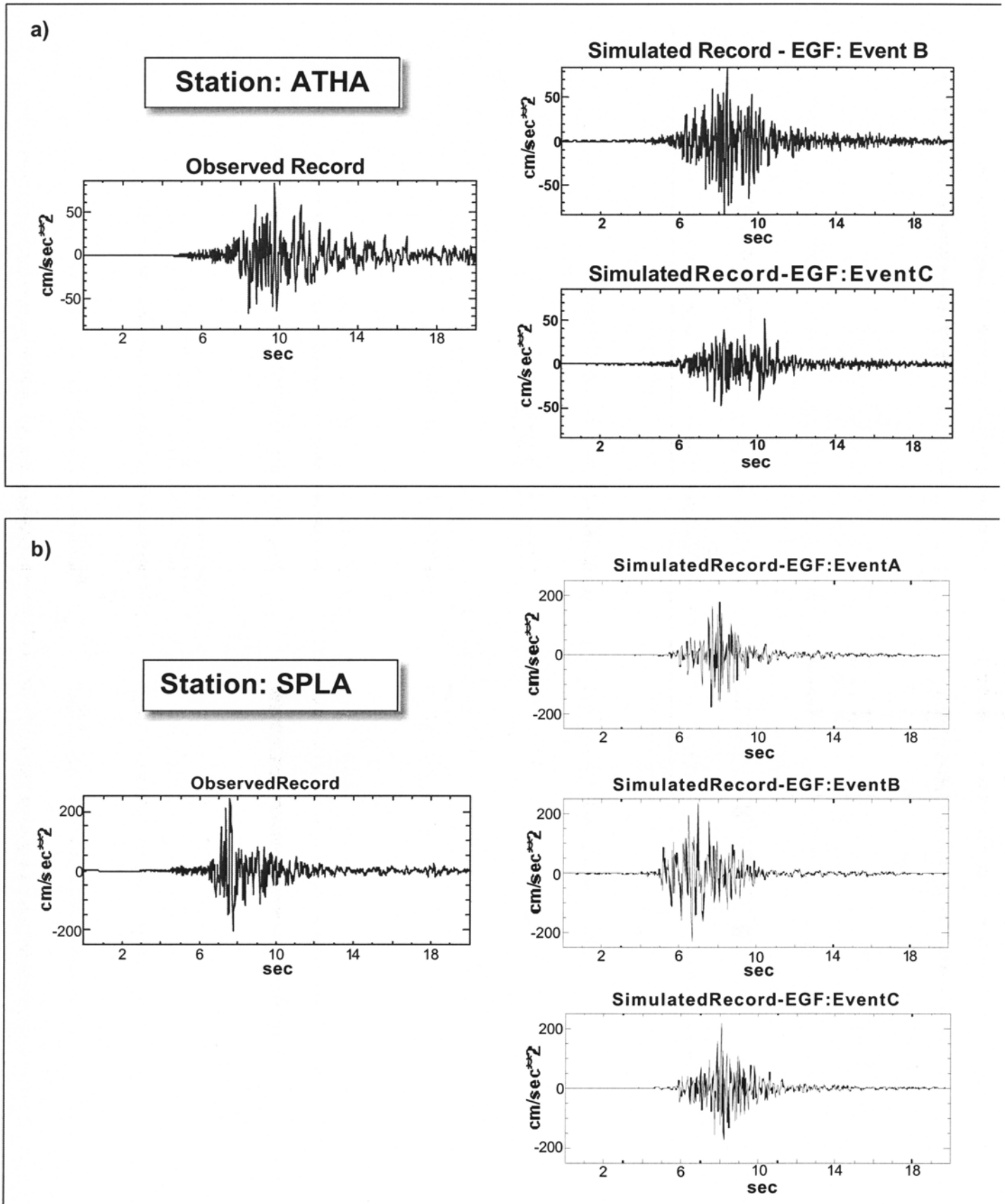
a)
Station: ATHA
Observed Record
Simulated Record - EGF: Event B
SimulatedRecord-EGF:EventC
cm/sec**2
sec
b)
Station: SPLA
ObservedRecord
SimulatedRecord-EGF:EventA
SimulatedRecord-EGF:EventB
SimulatedRecord-EGF:EventC

FIGURE 3

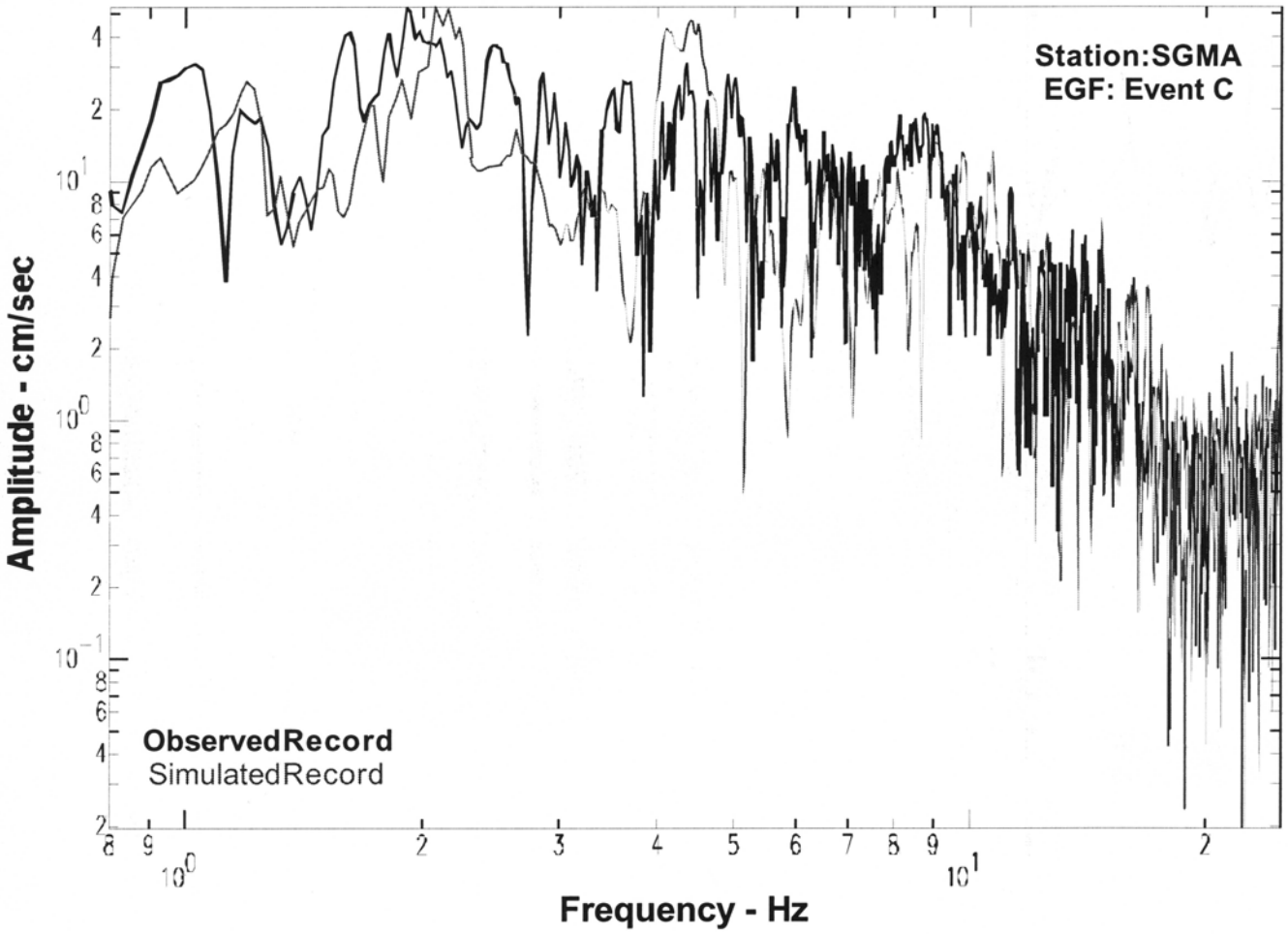
Station:SGMA
EGF: Event C
ObservedRecord
SimulatedRecord
Amplitude - cm/sec
Frequency - Hz

FIGURE 4

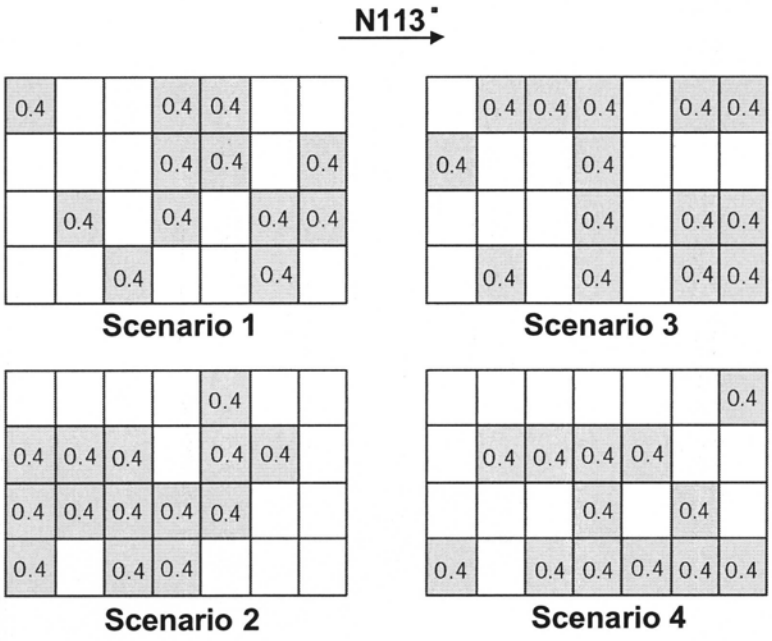
N113°
0.4 0.4 0.4 0.4 0.4 0.4 0.4 0.4 0.4 0.4 0.4 0.4 0.4 0.4 0.4 0.4 0.4 0.4 0.4 0.4
Scenario 1
0.4 0.4 0.4 0.4 0.4 0.4 0.4 0.4 0.4 0.4 0.4 0.4 0.4 0.4
Scenario 3
0.4 0.4 0.4 0.4 0.4 0.4 0.4 0.4 0.4 0.4 0.4 0.4 0.4 0.4 0.4 0.4 0.4 0.4 0.4 0.4
Scenario 2
0.4 0.4 0.4 0.4 0.4 0.4 0.4 0.4 0.4 0.4 0.4 0.4 0.4 0.4 0.4 0.4 0.4 0.4 0.4 0.4
Scenario 4

FIGURE 5

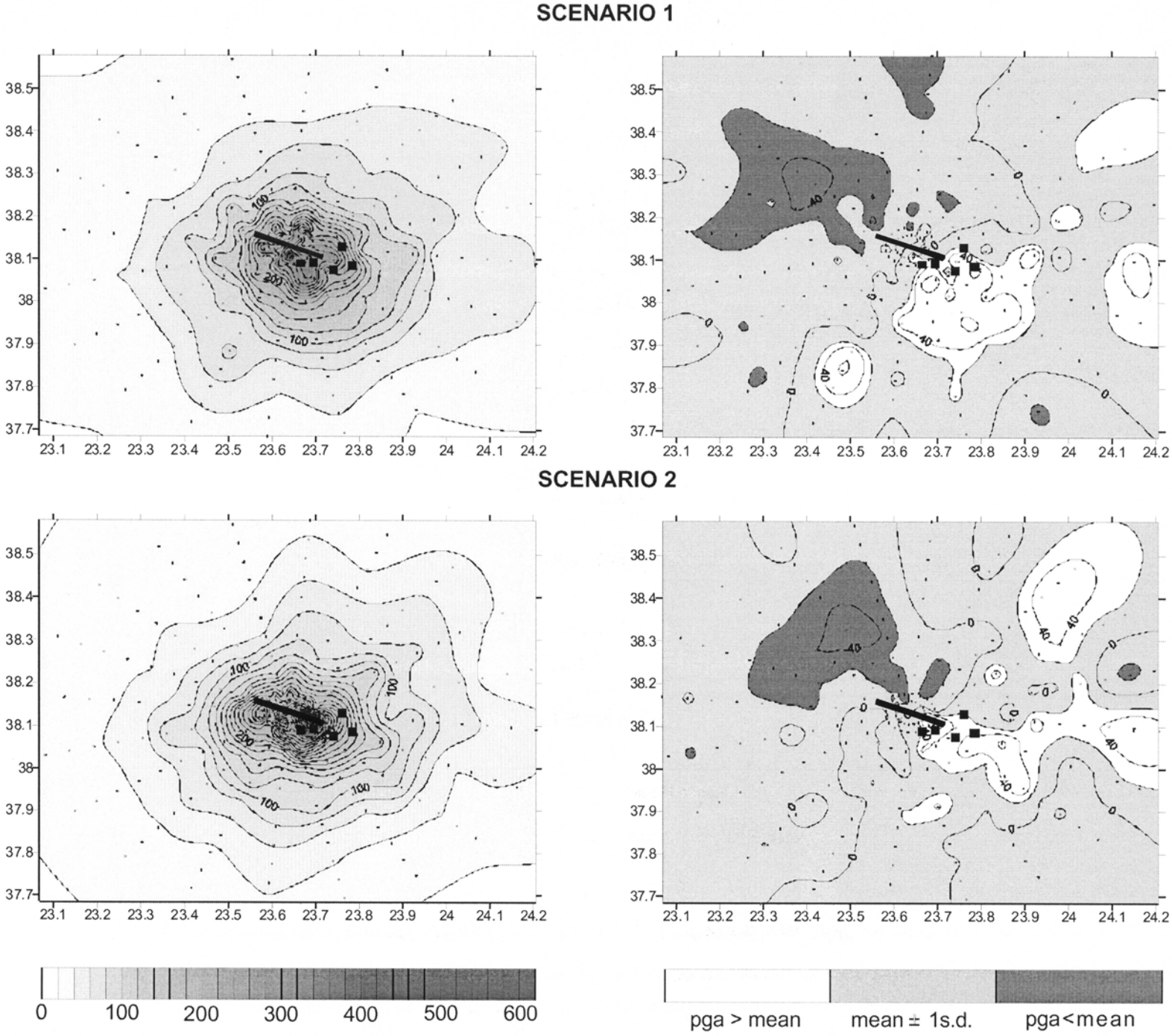
SCENARIO 1
SCENARIO 2
38.5
38.4
38.3
38.2
38.1
38
37.9
37.8
37.7
23.1 23.2 23.3 23.4 23.5 23.6 23.7 23.8 23.9 24 24.1 24.2
100
200
0
40
0 100 200 300 400 500 600
pga > mean
mean ± 1s.d.
pga<mean

FIGURE 6

SCENARIO 3

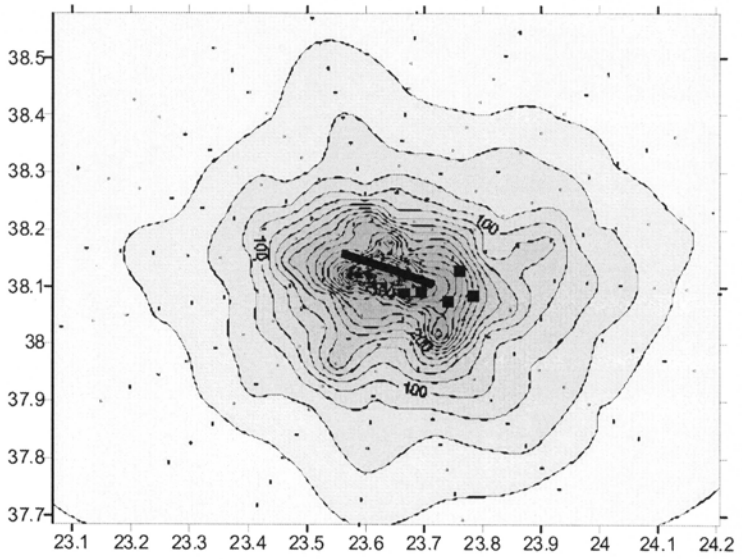

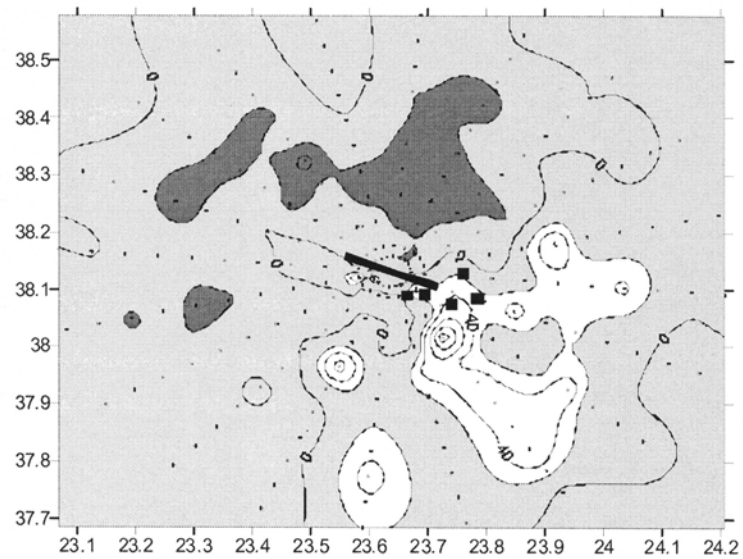

SCENARIO 4